

# Residual Stress Distributions in the Solid Solution Eutectic, $\text{Co}_{1-x}\text{Ni}_x\text{O}/\text{ZrO}_2(\text{CaO})$

L. N. Brewer,<sup>\*,†,‡</sup> R. A. Peascoe,<sup>§</sup> C. R. Hubbard,<sup>\*,§</sup> and V. P. Dravid<sup>\*,†</sup>

Department of Materials Science and Engineering, Northwestern University, Evanston, Illinois 60208  
High Temperature Materials Laboratory, Oak Ridge National Laboratory, Oak Ridge, Tennessee 37831

**This study investigates thermal mismatch stresses in the lamellar microstructure of the solid solution directionally solidified eutectic (DSE) oxide  $\text{Co}_{1-x}\text{Ni}_x\text{O}/\text{ZrO}_2(\text{CaO})$ . X-ray and neutron diffraction measurements were performed on isolated eutectic domains to measure the residual strain and stress tensors. Maximum principal residual stresses on the order of 1 GPa were recorded, with the  $\text{Co}_{1-x}\text{Ni}_x\text{O}$  and the  $\text{ZrO}_2(\text{CaO})$  phases maintaining states of tensile and compressive stress, respectively. The stress tensors for these materials are compared with measurements for similar DSE oxide systems and suggest that solid solution DSEs might be used to tailor the residual stress states in DSE composites.**

## I. Introduction

CONTROLLING and characterizing the residual stress state is an issue of importance for most classes of ceramic composites. Thermal expansion or phase transformation mismatches can generate residual stresses either on cooling during fabrication or during use by thermal cycling and/or diffusion. The usefulness or harmfulness of a residual stress state depends on the composite and its use. For most fiber-reinforced composites, residual stresses are undesirable because they inhibit fiber pullout during composite fracture.<sup>1</sup> However, residual stresses in laminate composites can be used to enhance crack deflection and interfacial delamination.<sup>2–4</sup>

A number of directionally solidified eutectic (DSE) oxide systems have been investigated as potential candidates for high-temperature composite materials (e.g.,  $\text{Y}_3\text{Al}_5\text{O}_{12}/\text{Al}_2\text{O}_3$ ,<sup>5</sup>  $\text{Al}_2\text{O}_3/\text{ZrO}_2$ ,<sup>6</sup> and  $\text{GdAlO}_3/\text{Al}_2\text{O}_3$ <sup>7</sup> among many others<sup>8,9</sup>). The materials range in microstructure from lamellar to fibrous to “Chinese script” morphologies. Since the eutectic composite is generally created by solidifying from the melt (usually greater than 1700°C), the potential exists for either helpful or harmful residual stress distributions to develop during cooling to room temperature from thermal expansion mismatch between the component phases of the composite.

Measurements of the residual strain in an assortment of DSE oxide composites have been made using diffraction- and

spectroscopy-based techniques. X-ray diffraction measurements of the residual strain state have been performed on the  $\text{NiO}/\text{ZrO}_2(\text{CaO})$  and  $\text{Y}_3\text{Al}_5\text{O}_{12}/\text{Al}_2\text{O}_3$  DSE.<sup>10,11</sup> Spectroscopy (fluorescence and Raman) measurements have been used to measure residual strains in the  $\text{Al}_2\text{O}_3/\text{ZrO}_2$  DSE.<sup>12</sup> In all these cases, the stresses were calculated from measured strains by using elasticity relationships. Previous measurements using X-ray diffraction demonstrated the presence of gigapascal-level residual stresses in the system,  $\text{NiO}/\text{ZrO}_2(\text{CaO}$  or  $\text{Y}_2\text{O}_3)$ . The maximum principal residual stresses at room temperature in the interfacial plane were tensile in  $\text{NiO}$  (+900 MPa on average) and compressive in  $\text{ZrO}_2$  (–1110 MPa on average).<sup>10</sup> The existence of these large stresses after cooling was attributed to strong interfacial bonding which stems from the electrostatic bonding between polar cation sheets ( $\text{Ni}^{2+}$  in the {111} plane,  $\text{Zr}^{4+}$  in the {100} plane) by an interfacial sheet of oxygen anions.

The solid solution DSE,  $\text{Co}_{1-x}\text{Ni}_x\text{O}/\text{ZrO}_2(\text{CaO})$ , is a novel materials system which has been recently developed for the study of the structure–property relationships controlling interfacial fracture in oxide composites.<sup>13</sup> This DSE is isostructural with  $\text{NiO}/\text{ZrO}_2(\text{CaO})$ , possessing a lamellar microstructure and a similar interfacial stacking sequence involving the {111} planes of  $\text{Co}_{1-x}\text{Ni}_x\text{O}$  and the {100} planes of  $\text{ZrO}_2(\text{CaO})$ . These structural similarities beg the question of whether or not the interfacial structure of the solid solution DSEs will support similar large stresses as are observed in  $\text{NiO}/\text{ZrO}_2(\text{CaO})$ . The thermal expansion coefficients of the  $\text{Co}_{1-x}\text{Ni}_x\text{O}$  phase have been observed to change with composition, which gives the expectation of a change in the residual stress state with composition.<sup>14</sup> A systematic change in the residual stress state with composition might provide a method for tailoring residual stresses and associated mechanical behavior in DSE composites.

In this paper, the residual stresses in the solid solution DSE are explored both theoretically and experimentally. The change in thermal mismatch stresses with composition is predicted with a simple elasticity model using experimental data for the thermal expansion coefficient. The residual strain tensors for both  $\text{Co}_{0.333}\text{Ni}_{0.666}\text{O}/\text{ZrO}_2(\text{CaO})$  and  $\text{Co}_{0.5}\text{Ni}_{0.5}\text{O}/\text{ZrO}_2(\text{CaO})$  are measured using X-ray diffraction. The residual strain tensor for  $\text{Co}_{0.5}\text{Ni}_{0.5}\text{O}/\text{ZrO}_2(\text{CaO})$  was independently measured using neutron diffraction. In all cases, the stress tensors were subsequently calculated using single-crystal elasticity data from the literature.

## II. Methodology

### (I) Calculation of Thermal Mismatch Stresses

As a first approximation, the lamellar microstructure of the solid solution DSEs (Fig. 1A) can be viewed as collection of plane-strain, fully constrained, isotropic, elastic slabs (Fig. 1B). Thermal mismatch stresses are calculated from the eutectic temperature to room temperature, assuming no creep or other relaxation during cooling.<sup>10</sup> The eutectic temperature is estimated to be ~1700°C for this system from previous work on the  $\text{NiO}/\text{CaO}$ <sup>15</sup> and

T. Parthasarathy—contributing editor

Manuscript No. 187425. Received October 12, 2001; approved September 27, 2002.

\*Member, American Ceramic Society.

This work was supported by the following sources: Grant No. NSF-DMR 9528488 (L.N.B. and V.P.D.) and DOD-NDSEG Fellowship (L.N.B.). This research was also sponsored by the Assistant Secretary for Energy Efficiency and Renewable Energy, Office of Transportation Technologies, as part of the High Temperature Materials Laboratory User Program, Oak Ridge National Laboratory, managed by UT-Battelle, LLC, for the U.S. Department of Energy under Contract No. DE-AC05-00OR22725.

<sup>†</sup>Northwestern University.

<sup>‡</sup>Present address: General Electric Global Research Center, Niskayuna, NY 12309.

<sup>§</sup>Oak Ridge National Laboratory.

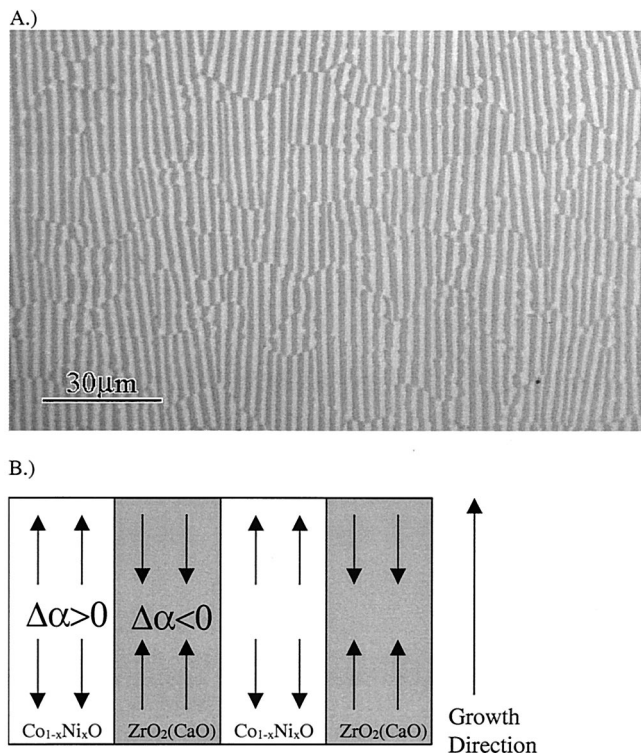


**Fig. 1.** Lamellar microstructures in  $\text{Co}_{1-x}\text{Ni}_x\text{O}/\text{ZrO}_2(\text{CaO})$ : (A) Optical micrograph from  $\text{Co}_{0.333}\text{Ni}_{0.666}\text{O}/\text{ZrO}_2(\text{CaO})$ ; the dark phase is  $\text{ZrO}_2(\text{CaO})$ , and the light phase is  $\text{Co}_{0.333}\text{Ni}_{0.666}\text{O}$ . (B) Schematic of ideal structure showing presence of residual stresses with arrows.

$\text{NiO}/\text{Y}_2\text{O}_3$ <sup>16</sup> eutectics. The in-plane thermal mismatch stresses for this geometry can be calculated as:

$$\sigma_p^A = \frac{\Delta\alpha \cdot \Delta T \cdot E^A}{1 - \nu^A} \left[ 1 + \left( \frac{t^A}{t^B} \right) \left( \frac{E^A}{1 - \nu^A} \right) \left( \frac{E^B}{1 - \nu^B} \right) \right]^{-1} \quad (1)$$

where  $\sigma_p^A$  is the residual stress of phase A on the plane parallel to the interface,  $\Delta\alpha \cdot \Delta T$  is the thermal mismatch strain between the two materials,  $E^i$  is Young's modulus of phase  $i$  (assumed to be isotropic),  $\nu^i$  is Poisson's ratio of phase  $i$ , and  $t^i$  is the thickness of layer  $i$ .<sup>4</sup> For the solid solution DSEs,  $E$  and  $\nu$  will be assumed to be independent of temperature and to follow a rule-of-mixtures behavior for the values of modulus for NiO and CoO. The values used in these calculations are derived from experimental measurements on NiO,<sup>17</sup> CoO,<sup>17</sup> and  $\text{ZrO}_2(\text{CaO})$ <sup>18</sup> (Table I). The parameter  $\alpha$  is the coefficient of thermal expansion (CTE). The variation of  $\alpha$  with composition in the  $\text{Co}_{1-x}\text{Ni}_x\text{O}$  phase has been measured previously from room temperature to 1500°C (Table II).<sup>14</sup> A variety of CTE values for stabilized zirconia have been reported in the literature (Table III).<sup>19–21</sup> The value of  $\alpha$  for fully stabilized  $\text{ZrO}_2(\text{CaO}-15\text{mol}\%)$  used here is  $10.4 \times 10^{-6}/\text{K}$ .<sup>22,23</sup>

**Table I.** Literature Values for the Elasticity of NiO, CoO, and  $\text{ZrO}_2(\text{CaO})$ <sup>†</sup>

	NiO	CoO	$\text{ZrO}_2(\text{CaO})$
C11 (GPa)	270	256	380
C12 (GPa)	125	144	120
C44 (GPa)	105	80	62
$E$ (GPa)	224	180	227
$\nu$	0.217	0.276	0.273

<sup>†</sup>Taken from Refs. 17 and 18.

**Table II.** Measured Values for the CTE of  $\text{Co}_{1-x}\text{Ni}_x\text{O}$  as a Function of CoO Content<sup>†</sup>

Mole fraction of CoO	Average CTE (1300–1500°C) ( $\times 10^{-6}/\text{K}$ )
0	16.7
0.33	20.4
0.66	20.5
1	18.1

<sup>†</sup>Taken from Ref. 14.

Due to the measured change in the CTE for the  $\text{Co}_{1-x}\text{Ni}_x\text{O}$  phase with temperature, a slightly more complex formulation for the thermal mismatch stresses can be used.

$$\sigma_p^A = \frac{E_p^A}{1 - \nu^A} \left[ 1 + \left( \frac{t^A}{t^B} \right) \left( \frac{E_p^A}{1 - \nu^A} \right) \left( \frac{E_p^B}{1 - \nu^B} \right) \right]^{-1} \int_{T_{\text{room}}}^{T_{\text{eutectic}}} \Delta\alpha(T) dT \quad (2)$$

Assuming identical phase fractions ( $t^A = t^B$ ) for simplicity, the thermal mismatch stresses must be opposite in sign but equal in magnitude to complete the force balance between phases.

## (2) Measurement of Thermal Mismatch Strains: X-ray and Neutron Diffractions

Samples of  $\text{Co}_{1-x}\text{Ni}_x\text{O}/\text{ZrO}_2(\text{CaO}-15\text{mol}\%)$  were directionally solidified using the optical floating zone method at the Laboratoire de Physico-Chimie de l'Etat, Université de Paris-Sud (Orsay, France), as has been described in more detail elsewhere.<sup>13</sup> Appropriate fractions of CoO, NiO,  $\text{ZrO}_2$ , and  $\text{CaCO}_3$  were combined into a powder mixture, calcined, isostatically pressed, and finally sintered. The sintered rods were directionally solidified using an NEC double ellipsoidal image furnace. Controlled atmospheres of Ar,  $\text{CO}_2$ , and air were used to suppress the formation of  $\text{Co}_3\text{O}_4$  during growth.

Thermal mismatch strains in the  $\text{Co}_{0.333}\text{Ni}_{0.666}\text{O}/\text{ZrO}_2(\text{CaO})$  and  $\text{Co}_{0.5}\text{Ni}_{0.5}\text{O}/\text{ZrO}_2(\text{CaO})$  eutectics were measured using single-crystal X-ray and neutron diffraction techniques. Eutectic domains of a single orientation or "eutectic single crystals" were isolated from the bulk eutectic by first identifying large domains of a single microstructural orientation on polished longitudinal sections of the bulk followed by removal of the domain with a low-speed diamond saw with further grinding and polishing. The resulting samples were  $\sim 300$ – $500 \mu\text{m}$  by  $300$ – $500 \mu\text{m}$  in cross section and  $\sim 0.5$ – $1 \text{ cm}$  in length with the lamellae oriented along the long axis of the specimen.

X-ray diffraction measurements were performed on a Scintag PTSTM four-circle goniometer ( $\phi$ ,  $\chi$ ,  $\omega$ ,  $2\theta$ ). The relevant diffractometer conditions are summarized in Table IV. The samples were oriented with respect to the laboratory reference frame (Fig. 2) with the  $X_1$  direction lying along the  $\phi$  rotation axis and the  $X_1$ – $X_3$  interfacial plane normal lying along the  $\chi$  rotation axis (within  $5^\circ$ ). X-ray pole figures were performed using the reflections of interest ( $\{113\}$  for  $\text{Co}_{1-x}\text{Ni}_x\text{O}$  and  $\{331\}$  for  $\text{ZrO}_2(\text{CaO})$ ) in addition to the more standard reflections of  $\{200\}$  and  $\{222\}$ . The  $\{113\}$  and  $\{331\}$  reflections were chosen because of their multiplicity (12 possible reflections in one hemisphere) and their high angular position for diffraction ( $>120^\circ$  for  $\text{CrK}\alpha$ ) for added strain sensitivity. After the diffraction normal was brought into the plane of

**Table III.** Literature Values for the CTE of Cubic Stabilized Zirconia as a Function of Stabilizer Type<sup>†</sup>

	Average CTE ( $\sim 20$ – $1000^\circ\text{C}$ ) ( $\times 10^{-6}/\text{K}$ )				
	Touloukian <sup>19</sup>	Terblanche <sup>21</sup>	Filatov <sup>22</sup>	Karaulov <sup>23</sup>	Lukin <sup>20</sup>
$\text{Y}_2\text{O}_3$ 12.9 (15%)	11.4 (9.3%)		11.2 (10%)		
CaO		10.4 (12%)	10.3 (15%)	10.7 (8%)	
MgO			11.8 (15%)	9.5 (8%)	

<sup>†</sup>Values in parentheses are mole percent levels of the stabilizer.

**Table IV. X-ray Diffractometer Conditions for Residual Strain Measurement**

Scintag PTS four-circle goniometer	
Anode power	Cr X-ray tube: 1.4 kW; 40 kV; 35 mA
Detector/filters	Intrinsic Ge detector, PHA rejects CrK $\beta$ line
Radiation	CrK $\alpha$ , $\lambda = 2.2897 \text{ \AA}$
Incident slit	0.55°, 2 mm diameter short pinhole
divergence	collimator
Receiving divergence	<1.9°, radial divergence limiting Soller slits
Source-to-sample distance	290 mm
Sample-to-back-slit distance	290 mm
Scan rates	0.02° 2 $\theta$ /s, >500 cps at peak

the detector, a rocking curve in 2 $\theta$  for that ( $hkl$ ) reflection was recorded.

To complete the strain measurement ( $(d - d_0)/d_0$ ), it was necessary to measure a strain-free standard. This was accomplished by performing X-ray powder diffraction on a pulverized section of the eutectic from an adjacent section of the isolated crystal in the bulk to minimize compositional variation. Small amounts of NBS standard silicon (SRM6406) were added to the crushed powder as an internal calibration standard. The powders were crushed under liquid nitrogen to suppress plastic deformation in the  $\text{Co}_{1-x}\text{Ni}_x\text{O}$  phase that could lead to peak broadening. The powders were not annealed due to the possibility of change in the point defect concentration and in the composition from the nucleation of the  $\text{Co}_3\text{O}_4$  spinel phase. The powder lattice parameters were also measured on a Scintag PTS<sup>TM</sup> diffractometer under the same conditions as the strain measurements but with scans (2 $\theta$ ) from 40° to 160° at scan rates of 0.02°/2.3 s. The strain-free lattice parameters were calculated using a least-squares-refinement approach in the commercially available Jade software package<sup>24</sup> and are given in Table V.

**Table V. Measured Strain-Free Lattice Parameters by X-ray Diffraction**

	Lattice parameter ( $\text{\AA}$ )	
	$\text{Co}_{1-x}\text{Ni}_x\text{O}$	$\text{ZrO}_2(\text{CaO})$
$\text{Co}_{0.333}\text{Ni}_{0.666}\text{O}/\text{ZrO}_2(\text{CaO})$	$4.2034 \pm 0.0015$	$5.1292 \pm 0.0027$
$\text{Co}_{0.5}\text{Ni}_{0.5}\text{O}/\text{ZrO}_2(\text{CaO})$	$4.2177 \pm 0.0011$	$5.1271 \pm 0.0032$

The neutron diffraction measurements were similar in method to the X-ray diffraction measurements with several important differences. The neutron measurements were performed on beam line HB-2 in the high-flux isotope reactor (HFIR) at Oak Ridge National Laboratory. A sample of  $\text{Co}_{0.5}\text{Ni}_{0.5}\text{O}/\text{ZrO}_2(\text{CaO})$  was mounted on a Huber two-circle goniometer with the long axis of the sample (parallel to lamellae) along the  $\phi$  axis. The {222} reflections were used to measure strains in the  $\text{Co}_{0.5}\text{Ni}_{0.5}\text{O}$  phase, and {400} reflections were used to measure strains in the  $\text{ZrO}_2(\text{CaO})$  phase as a function of  $\phi$  and  $\chi$ . The position of the 2 $\theta$  detector arm was calibrated with a powder Ni standard and a powder  $\text{ZrO}_2(\text{CaO})$  standard. The X-ray diffraction measured values for the strain-free lattice parameters for the  $\text{Co}_{0.5}\text{Ni}_{0.5}\text{O}$  and  $\text{ZrO}_2(\text{CaO})$  phases were used to calculate strain from the neutron diffraction measurements. Table VI summarizes the neutron diffractometer conditions.

The strain tensor  $\epsilon_{kl}$  was calculated (Eq. (3)) by combining measured strains ( $e_{33}^{\phi\chi}$ ) from measured  $d$ -spacings using as many reflections ( $d_{hkl}^{\phi\chi}$ ) as possible with the strain-free lattice parameter ( $d_0$ ) in an overdetermined system of linear equations (greater than six  $d$ -spacings).<sup>25</sup>

$$e_{33}^{\phi\chi} = \frac{d_{hkl}^{\phi\chi} - d_0}{d_0} \quad (3)$$

This tensor was transformed into the sample coordinate system ( $\epsilon_{kl}$ ) using direction cosines ( $\alpha_{ij}$ ) (Eq. (4)).

$$e_{33}^{\phi\chi} = a_{3k}a_{3l}\epsilon_{kl} \quad (4)$$

A generalized least-squares routine was used to fit this tensor to the strain data using the singular variable decomposition (SVD) algorithm.<sup>26</sup> The error values propagated through this calculation were based on estimates of the standard error from the lattice parameter measurements and are quoted in units of strain.

The stresses ( $\sigma_{ij}$ ) in this paper were calculated from the measured strains ( $\epsilon_{kl}$ ) by relating them through basic elasticity relationships<sup>27</sup> using room-temperature, single-crystal elasticity data ( $C_{ijkl}$ ) from the literature for both phases (Table I).<sup>17,18</sup>

$$\sigma_{ij} = C_{ijkl}\epsilon_{kl} \quad (5)$$

Elasticity values for the  $\text{Co}_{1-x}\text{Ni}_x\text{O}$  phase were approximated as a rule of mixtures between CoO and NiO. Values for elasticity in  $\text{ZrO}_2(\text{CaO})$  were taken for the nearest composition to the nominal composition for these samples. Errors for the stress tensors were propagated using only the error estimates on the strain tensors due to a lack of error estimates on the elasticity data in the literature sources.

**Table VI. High-Flux Isotope Reactor (HFIR) HB-2 Beam Line Neutron Diffractometer Conditions for Residual Stress Measurements**

Beam line HB-2; Huber two-circle goniometer	
Detector	Position-sensitive detector (PSD)
Radiation	$\lambda = 1.652 \text{ \AA}$ neutrons
Incident divergence	1-mm pinhole collimator 70 mm from sample
Receiving divergence	0.25°, radial divergence slit
Sample-to-detector distance	80 mm

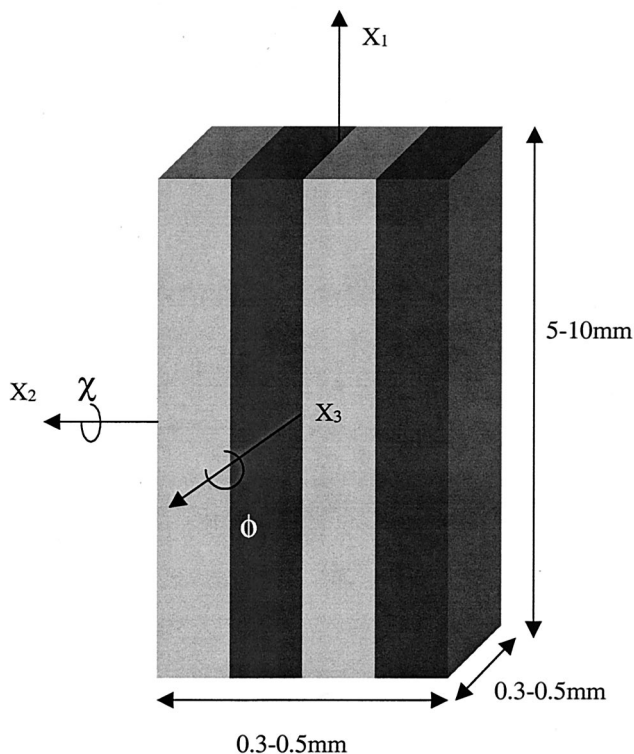


**Fig. 2.** Sample and diffractometer coordinate system for X-ray residual stress measurements. Note that the interface plane is given by the  $X_1 - X_3$  plane.

### III. Results

#### (1) Expected Thermal Mismatch Stresses

The insertion of experimentally measured thermal expansion data for the  $\text{Co}_{1-x}\text{Ni}_x\text{O}$  and  $\text{ZrO}_2(\text{CaO})$  phases into Eq. (2) results in the prediction of large thermal mismatch stresses across the solid solution (Fig. 3). In addition, these stresses in the middle of the solid solution may increase by as much as 30% over those in  $\text{NiO}/\text{ZrO}_2(\text{CaO})$  due to an increase of the thermal expansion coefficient with temperature for the middle compositions. This has been attributed previously to an increased ease of formation for point defects in the solid solution as compared with the end compositions  $\text{CoO}$  and  $\text{NiO}$ .<sup>14</sup> It is important to note the difference in the stress prediction between a constant CTE and one that changes with temperature. In particular, the use of a constant CTE value greatly overestimates the expected residual stress for the end compositions  $\text{NiO}/\text{ZrO}_2(\text{CaO})$  and  $\text{CoO}/\text{ZrO}_2(\text{CaO})$ .

#### (2) X-ray and Neutron Diffraction Strain and Stress Tensors

The residual strain and stress tensors obtained by X-ray diffraction for the  $\text{Co}_{0.333}\text{Ni}_{0.666}\text{O}/\text{ZrO}_2(\text{CaO})$  and  $\text{Co}_{0.5}\text{Ni}_{0.5}\text{O}/\text{ZrO}_2(\text{CaO})$  eutectics are shown in Appendixes A and B, respectively. The principal stresses in each tensor are an order of magnitude larger than the off-axis stresses ( $\sigma_{ij}$ ,  $i \neq j$ ) and their respective error estimates. In the plane of the interface, the stresses are tensile for the  $\text{Co}_{1-x}\text{Ni}_x\text{O}$  phase and compressive for the  $\text{ZrO}_2(\text{CaO})$  phase, as expected.

The residual strain and stress tensors for  $\text{Co}_{0.5}\text{Ni}_{0.5}\text{O}/\text{ZrO}_2(\text{CaO})$  measured by neutron diffraction are shown in Appendix C. Strain measurements for the  $\text{ZrO}_2(\text{CaO})$  phase were unsuccessful due to the weak neutron scattering structure factors for  $\text{ZrO}_2$ .<sup>28</sup> The strain and stress tensors for the  $\text{Co}_{1-x}\text{Ni}_x\text{O}$  phase are in qualitative agreement with those from the X-ray measurement but are larger in magnitude. Again the magnitude of the principal stresses is an order of magnitude greater than the off-axis stresses or the measurement errors.

#### (3) Force Balances

As a check on the physical validity of the results, we have calculated the force balance between phases using the idealized slab model for the microstructure. In this force balance, the sum of the forces along any principal direction should sum to zero (neglecting off-axis stresses) (Eqs. (6) and (7)). For the interfacial constraint stresses, the magnitude of the stresses is weighted by the area fraction (identical to the volume fraction for phases of equal through thickness) of each phase.

$$\sigma_i^{\text{CoNiO}} \cdot V_{f_{\text{CoNiO}}} = -\sigma_i^{\text{ZrO}_2} \cdot V_{f_{\text{ZrO}_2}} \quad (6)$$

$$\frac{\sigma_i^{\text{CoNiO}}}{\sigma_i^{\text{ZrO}_2}} = -\frac{V_{f_{\text{ZrO}_2}}}{V_{f_{\text{CoNiO}}}} \quad (7)$$

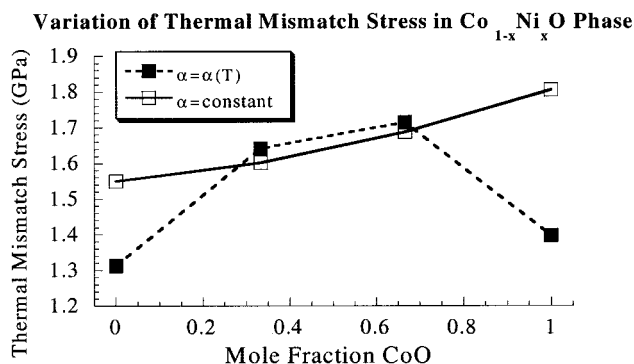


Fig. 3. Predicted residual stresses in the  $\text{Co}_{1-x}\text{Ni}_x\text{O}/\text{ZrO}_2(\text{CaO})$  DSE due to thermal mismatch.

The volume fractions for the phases in each specimen were measured by calculating the area fraction of each phase from SEM images of transverse sections of DSEs and assuming an identical through-thickness dimension for each phase. The stress balances for each phase are listed in Table VII. The stress balances are within measurement error of the negative of the volume fraction ratio (Eq. (7)) for  $\sigma_{11}$ ,  $\sigma_{33}$ , and their average in each composition. Note the particularly good agreement in the  $\sigma_{11}$  balance as it is the direction for which the microstructural relationship to the goniometer is unambiguous. The values for  $\sigma_{22}$  are unexpectedly large and of unexpected sign, given that this is the principal direction for Poisson-generated stresses. The force balance ratio for  $\sigma_{22}$  is within the error margin of a perfect force balance ( $-1.0$ ) for  $\text{Co}_{0.333}\text{Ni}_{0.666}\text{O}/\text{ZrO}_2(\text{CaO})$ , but not for  $\text{Co}_{0.5}\text{Ni}_{0.5}\text{O}/\text{ZrO}_2(\text{CaO})$ . The force balance for the neutron diffraction results was not calculated due to a lack of data from the  $\text{ZrO}_2(\text{CaO})$  phase.

### IV. Discussion

The stress tensors are both self-consistent (dominance of principal stresses, force balances, etc.) and are also fairly consistent between techniques (X-ray versus neutron diffraction). The agreement between the neutron and X-ray results is important because it shows that surface relaxation of the stresses is most likely a low-level artifact in these measurements. The  $\text{CrK}\alpha$  radiation used in the X-ray experiment has a penetration depth (for 90% attenuation) of  $\sim 25 \mu\text{m}$ . This depth is several times the lamellar width but still fairly close to the surface. The neutron beam completely penetrates the sample, sampling the entire volume and thus averaging over the whole crystal, likely eliminating any type of surface relaxation aberration. The seeming lack of surface relaxation observed is most likely due to the fact that microcompatibility stresses are being measured as opposed to some sort of macrostress that would more readily relax near the surface.<sup>25</sup> The larger observed stresses in the neutron diffraction measurements may be from radial, macroscopic strain gradients in the bulk crystal.

The strain and stress values reported may also be affected by the measured value of the “strain-free” lattice parameter. Small variations in  $d_0$  can greatly affect the accuracy of the strain measurement, quickly negating its validity. In this case, the two greatest possible artifacts for the measurement of  $d_0$  are compositional fluctuations and incomplete relaxation of residual strains within the standard. As noted above, strain-free specimens were taken from material directly adjacent ( $\sim 300 \mu\text{m}$  radially) from the strained samples at the same longitudinal position in the bulk eutectic to try to minimize any compositional fluctuations associated with segregation along the eutectic growth. Compositional fluctuations could bias the absolute accuracy of the results in either direction (more or less strain). Incomplete relaxation of strain would come from particles in the pulverized eutectic in which the lamellae are still well-bonded. High-temperature annealing would only partially relax residual strains (strains could still develop from the onset of recovery to room temperature) and would most likely change the point defect concentration and perhaps the composition (due to volatilization and phase transformation of  $\text{CoO}$  to  $\text{Co}_3\text{O}_4$ ). An incomplete relaxation can only *underestimate* the measured strain if the strain free standard is measured for both phases simultaneously. We therefore believe that the strains observed in this study are at least as large as reported and are not overestimated

Table VII. Force Equilibrium Ratios for Stress Tensors

	$\text{Co}_{0.333}\text{Ni}_{0.666}\text{O}/\text{ZrO}_2(\text{CaO})$	$\text{Co}_{0.5}\text{Ni}_{0.5}\text{O}/\text{ZrO}_2(\text{CaO})$
$V_{f_{\text{Co}_{1-x}\text{Ni}_x\text{O}}}^{\text{Co}_{1-x}\text{Ni}_x\text{O}}$ (%)	$52.7 \pm 11.7$	$58.0 \pm 10.9$
$V_{f_{\text{ZrO}_2(\text{CaO})}}^{\text{ZrO}_2(\text{CaO})}$ (%)	$47.3 \pm 13.3$	$42.0 \pm 9.1$
Force ratio expected	$-0.90 \pm 0.36$	$-0.72 \pm 0.38$
$\sigma_{11}$ ratio observed	$-1.02 \pm 0.12$	$-0.69 \pm 0.13$
$\sigma_{33}$ ratio observed	$-0.80 \pm 0.11$	$-1.11 \pm 0.19$
Average ratio observed	$-0.91 \pm 0.13$	$-0.90 \pm 0.18$
$\sigma_{22}$ ratio observed	$-1.19 \pm 0.16$	$-0.56 \pm 0.23$

but may be underestimated. Since the above force balance ratios are approximately equal and within the estimated errors, the independently measured  $d_0$  values are likely reasonably accurate and, hence, the calculated strains and stresses as well.

The large ( $\geq 1$  GPa) principal residual stresses can be readily interpreted in terms of the microstructure. The large, positive values of stress along the  $X_1$  and  $X_3$  principal directions demonstrate a large value of tensile stress in the plane of the interface in the  $\text{Co}_{1-x}\text{Ni}_x\text{O}$  phase (large and compressive for  $\text{ZrO}_2(\text{CaO})$ ). The magnitude of the stresses points to strong interfacial bonding in the solid solution DSEs, as might be hypothesized from their crystallographic orientation relationships. This result is important because it demonstrates that the effect of adding  $\text{CoO}$  to the solid solution does not relax the interfacial constraint on the lamellae. However, the observation of large stresses in the  $X_2$  direction with the same sign as that along  $X_1$  and  $X_3$  is not in keeping with the simple microstructural picture in Figs. 1(B) and 2. In addition, the force balance for the  $X_2$  direction is not achieved for the  $\text{Co}_{0.5}\text{Ni}_{0.5}\text{O}/\text{ZrO}_2(\text{CaO})$  crystal. The  $X_2$  principal stress in Figs. 1(B) and 2 should be a Poisson-generated stress which is smaller than and opposite in sign to the  $X_1$  and  $X_3$  principal stresses. In contrast to the simple slab model, the real microstructure of these samples consists of domains of lamellae which are all oriented in a similar direction but are interrupted every 20–30  $\mu\text{m}$  (Fig. 1(A)). These interruptions in lamellar structure are called lamellar growth faults in the crystal growth literature and stem from changes in the fusion zone volume during growth.<sup>29</sup> This faulted structure means that at every fault a  $\text{Co}_{1-x}\text{Ni}_x\text{O}/\text{ZrO}_2(\text{CaO})$  interface forms in the  $X_2$ – $X_3$  plane, which would generate the same sorts of strains as those observed in the  $X_1$ – $X_3$  plane, possibly giving a finite value of the same sign for the  $X_2$  principal strain.

The large residual stresses measured in this work are in keeping with those measured in other ceramic DSEs. Previous work on the  $\text{NiO}/\text{ZrO}_2(\text{CaO})$  system with X-rays demonstrated residual stresses with the same sign and general magnitude as have been observed here.<sup>10</sup> Similar studies with X-rays on the  $\text{YAG}/\text{Al}_2\text{O}_3$  DSE have shown much lower stresses (barely above the measurement threshold) due to the small difference in CTE between YAG and alumina.<sup>11</sup> Piezospectroscopic ( $\text{Cr}^{3+}$  luminescence and Raman) studies on  $\text{Al}_2\text{O}_3/\text{ZrO}_2$  DSE oxides revealed residual stresses due to thermal mismatch in the range of 300 MPa to 4 GPa.<sup>12</sup> For samples with monoclinic  $\text{ZrO}_2$ , the  $\text{ZrO}_2$  phase was in compression and the  $\text{Al}_2\text{O}_3$  phase was in tension. For samples with  $\text{Y}_2\text{O}_3$ -stabilized cubic  $\text{ZrO}_2$ , the  $\text{ZrO}_2$  phase was in tension and the  $\text{Al}_2\text{O}_3$  phase was in compression due to the increased CTE value from monoclinic to cubic  $\text{ZrO}_2$ . Calculations have been made for the residual stresses in the  $\text{MoSi}_2/\text{Mo}_5\text{Si}_3$  DSE that predict thermal mismatch residual stresses on the order of 600 MPa to 2.5 GPa.<sup>30</sup>

The ability of ceramic DSEs to retain such large stresses without relaxation on cooling reveals a great deal about the mechanical nature of the interface and the microstructure of these materials. First and foremost, these large stresses demonstrate the extremely well-bonded nature of the internal interfaces in DSEs, as it is the interfacial constraint which gives rise to the thermal mismatch stresses. Interfacial constraint in  $\text{NiO}/\text{ZrO}_2$  has been explained with electrostatic interfacial bonding as its source.<sup>10,31</sup> It has been observed that the interfacial structure of the solid solution eutectics is different

from that of  $\text{NiO}/\text{ZrO}_2$  as evidenced by a changing growth orientation relationship.<sup>13</sup> However, the nature of the interfacial planes ( $\{111\}$  for  $\text{Co}_{1-x}\text{Ni}_x\text{O}$  and  $\{100\}$  for  $\text{ZrO}_2(\text{CaO})$ ) remains the same for all compositions, and it is quite possible that electrostatic bonding plays a dominant role in interfacial adhesion for these materials as it does in  $\text{NiO}/\text{ZrO}_2(\text{CaO})$ . Another observation about stresses of these magnitudes is the level of strain supported without cracking. For these measurements and the measurements on  $\text{NiO}/\text{ZrO}_2(\text{CaO})$ , elastic strains in excess of 0.2% were readily observed, while strains in excess of  $\sim 0.15\%$  often cause failure in bulk, polycrystalline ceramics. The support of such large strains is most likely due to the lack of significant flaws in the DSE microstructure as grown from the melt. Lastly, the measured stresses ( $\sim 1$  GPa) are well in excess of the measured yield strengths ( $\sim 100$  MPa) for single crystals of  $\text{NiO}$  and  $\text{CoO}$  in compression.<sup>32,33</sup> To understand the generation of gigapascal stresses in this phase, it is necessary to follow the development of these stresses on cooling. As will be discussed below, thermal mismatch stresses will actually not develop until the sample is cooled to some fraction of the melting point (e.g., 70%). Below this temperature, the thermal mismatch stresses will increase as the sample cools until the yield point is exceeded. The  $\text{Co}_{1-x}\text{Ni}_x\text{O}$  materials are known to deform at high temperature by dislocation climb.<sup>34</sup> With further cooling, one might expect that these materials will strain harden very quickly until the upper yield point is increased to levels on the order of gigapascals, capable of supporting the observed residual stresses. This sort of deformation sequence, resulting in residual stresses larger than the yield stress, has been observed in thermal cycling behavior of metal matrix composites.<sup>35</sup>

In light of the simple model used here and previous residual stress measurements on  $\text{NiO}/\text{ZrO}_2$ , changes in composition do appear to control the level of residual stress in the system in a somewhat predictable fashion (Table VIII). As predicted, the solid solution composition stresses are significantly larger than those observed in  $\text{NiO}/\text{ZrO}_2$ . The increase in stress magnitude in the solid solution DSEs over those observed in  $\text{NiO}/\text{ZrO}_2$  can be explained by the increase in CTE for the  $\text{Co}_{1-x}\text{Ni}_x\text{O}$  phase with increasing  $\text{CoO}$ . This increase in stress suggests that composition might be used as a variable to tailor the residual stress level in solid solution DSEs. Despite the general increase in measured stresses compared with  $\text{NiO}/\text{ZrO}_2(\text{CaO})$ , the X-ray-diffraction-measured stresses in the  $\text{Co}_{0.333}\text{Ni}_{0.666}\text{O}/\text{ZrO}_2(\text{CaO})$  sample are slightly larger than those for the  $\text{Co}_{0.5}\text{Ni}_{0.5}\text{O}/\text{ZrO}_2(\text{CaO})$  sample, which is the opposite trend from what is predicted. However, the neutron diffraction data do show measurably larger stresses in the  $\text{Co}_{0.5}\text{Ni}_{0.5}\text{O}/\text{ZrO}_2(\text{CaO})$  sample that are close to the predicted levels.

The simple calculation made at the beginning of this paper is instructive in predicting the order of magnitude of the thermal mismatch stresses. However, the model ignores several important physical parameters that may explain the difference between the measured values and the model's predictions. The choice of the eutectic temperature as the point of onset for stress development appears to have overestimated the residual stress levels. Stresses will only develop at a lower temperature, e.g., 60–70%, of the eutectic point. This lower onset temperature may explain the systematically lower values for the measured residual stresses compared with the predicted stresses. The model also neglects any macrostresses that might develop due to a thermal gradient from the outside of the sample to the inside during growth. A possibly large underestimation of the residual stresses might come from

**Table VIII. Comparison between Experimental versus Calculated  $X_1$ – $X_3$  Plane Residual Stresses**

	$\text{Co}_{0.5}\text{Ni}_{0.5}\text{O}/\text{ZrO}_2$						$\text{Co}_{0.3}\text{Ni}_{0.6}\text{O}/\text{ZrO}_2$		$\text{NiO}/\text{ZrO}_2^\ddagger$	
	X-ray data		Neutron data		Model <sup>†</sup>		X-ray data			
	$\text{Co}_{0.5}\text{Ni}_{0.5}\text{O}$	$\text{ZrO}_2$	$\text{Co}_{0.5}\text{Ni}_{0.5}\text{O}$	$\text{ZrO}_2$	$\text{Co}_{0.5}\text{Ni}_{0.5}\text{O}$	$\text{ZrO}_2$	$\text{Co}_{0.3}\text{Ni}_{0.6}\text{O}$	$\text{ZrO}_2$	$\text{NiO}$	$\text{ZrO}_2$
$\sigma_{11}$ (MPa)	1140 $\pm$ 130	–1650 $\pm$ 130	1050 $\pm$ 40	–	1677	–1677	1370 $\pm$ 120	–1340 $\pm$ 50	929 $\pm$ 20	–840 $\pm$ 50
$\sigma_{33}$ (MPa)	1030 $\pm$ 90	–930 $\pm$ 80	1140 $\pm$ 30	–	1677	–1677	1360 $\pm$ 150	–1700 $\pm$ 40	927 $\pm$ 20	–1045 $\pm$ 60

<sup>†</sup>Based on the assumption of equal volume fractions. <sup>‡</sup>Original paper uses  $\sigma_{22}$  as  $\sigma_{11}$  used here.<sup>10</sup>

only a mild overestimation in the coefficient of thermal expansion (CTE) for the  $\text{ZrO}_2(\text{CaO})$  phase. As noted in Table III, the CTE of stabilized zirconia varies considerably with the amount and type of stabilizer used. Furthermore, the assumption of the temperature independence of Young's modulus is most likely not correct; however, substantial data on this parameter for the present materials are not currently available. All these observations suggest that while the simple model used here and elsewhere has been helpful for predicting stress magnitudes, a more refined model is necessary for actually predicting the effects of process variables on thermal mismatch residual stresses in this and related DSE oxide systems.

## V. Conclusions

The residual stress tensors in the solid solution DSE oxides,  $\text{Co}_{1-x}\text{Ni}_x\text{O}/\text{ZrO}_2(\text{CaO})$  ( $x = 0.5$  and  $0.666$ ), have been measured using single-crystal X-ray and neutron diffraction techniques. In the plane of the lamellae, residual stresses of 1 GPa and greater were observed with both techniques for these compositions. The large stresses in the interfacial plane point to the remarkable strength of interfacial constraint in this system, as has been previously observed in  $\text{NiO}/\text{ZrO}_2(\text{CaO})$ . The residual stresses for the solid solution DSEs are larger than those in  $\text{NiO}/\text{ZrO}_2(\text{CaO})$ , as predicted by a simple elastic slab model. The increase in residual stress is attributed to the increased thermal expansion coefficient of the  $\text{Co}_{1-x}\text{Ni}_x\text{O}$  phase with increasing CoO fraction. The ability to control residual stress levels using solid solutions may allow for further tailoring of mechanical behavior in DSE composites.

## Acknowledgment

L.N.B. thanks Dr. Y. Gao and Dr. N. Bhate for their helpful input on this manuscript.

## Appendix A

### Strain Tensors Measured by X-ray Diffraction

#### Strain Tensors for $\text{Co}_{0.5}\text{Ni}_{0.5}\text{O}/\text{ZrO}_2(\text{CaO})$

##### (a) $\text{ZrO}_2(\text{CaO})$ {331}

$$\varepsilon_{ij} = \begin{pmatrix} -3.96 & -0.03 & -0.05 \\ -0.03 & 0.04 & 0.004 \\ -0.05 & 0.004 & -1.12 \end{pmatrix} \\ \pm \begin{pmatrix} 0.28 & 0.13 & 0.07 \\ 0.13 & 0.08 & 0.06 \\ 0.07 & 0.06 & 0.08 \end{pmatrix} \cdot 10^{-3}$$

##### (b) $\text{Co}_{0.5}\text{Ni}_{0.5}\text{O}$ {113}

$$\varepsilon_{ij} = \begin{pmatrix} 3.56 & -0.21 & -0.01 \\ -0.21 & -1.607 & 0.05 \\ -0.01 & 0.05 & 2.92 \end{pmatrix} \\ \pm \begin{pmatrix} 0.38 & 0.10 & 0.08 \\ 0.10 & 0.19 & 0.09 \\ 0.08 & 0.09 & 0.07 \end{pmatrix} \cdot 10^{-3}$$

#### Strain Tensors for $\text{Co}_{0.333}\text{Ni}_{0.666}\text{O}/\text{ZrO}_2(\text{CaO})$

##### (c) $\text{ZrO}_2(\text{CaO})$ {331}

$$\varepsilon_{ij} = \begin{pmatrix} -2.76 & 0.87 & -0.02 \\ 0.87 & -0.34 & -0.573 \\ -0.02 & -0.573 & -3.12 \end{pmatrix} \\ \pm \begin{pmatrix} 0.08 & 0.15 & 0.07 \\ 0.15 & 0.05 & 0.06 \\ 0.07 & 0.06 & 0.06 \end{pmatrix} \cdot 10^{-3}$$

##### (d) $\text{Co}_{0.333}\text{Ni}_{0.666}\text{O}$ {113}

$$\varepsilon_{ij} = \begin{pmatrix} 2.88 & -0.57 & -0.85 \\ -0.57 & 1.742 & 0.23 \\ -0.85 & 0.23 & 2.92 \end{pmatrix} \\ = \begin{pmatrix} 0.18 & 0.09 & 0.16 \\ 0.09 & 0.22 & 0.06 \\ 0.16 & 0.06 & 0.33 \end{pmatrix} \cdot 10^{-3}$$

## Appendix B

### Stress Tensor Calculated from X-ray Diffraction Strain Tensor

#### Stress Tensors for $\text{Co}_{0.5}\text{Ni}_{0.5}\text{O}/\text{ZrO}_2(\text{CaO})$

##### (a) $\text{ZrO}_2(\text{CaO})$

$$\sigma_{ij} = \begin{pmatrix} -1634 & -3 & -5 \\ -3 & -594 & 0.3 \\ -5 & 0.3 & -896 \end{pmatrix} \\ \pm \begin{pmatrix} 125 & 82 & 8 \\ 82 & 75 & 7 \\ 8 & 7 & 75 \end{pmatrix} \text{ (MPa)}$$

##### (b) $\text{Co}_{0.5}\text{Ni}_{0.5}\text{O}$

$$\sigma_{ij} = \begin{pmatrix} 1113 & -20 & -1 \\ -20 & 452 & 5 \\ -1 & 5 & 1032 \end{pmatrix} \\ + \begin{pmatrix} 134 & 22 & 16 \\ 22 & 107 & 11 \\ 16 & 11 & 90 \end{pmatrix} \text{ (MPa)}$$

#### Stress Tensors for $\text{Co}_{0.333}\text{Ni}_{0.666}\text{O}/\text{ZrO}_2(\text{CaO})$

##### (c) $\text{ZrO}_2(\text{CaO})$

$$\sigma_{ij} = \begin{pmatrix} -1464 & 81 & -2 \\ 81 & -835 & -53 \\ -2 & -53 & -1558 \end{pmatrix} \\ \pm \begin{pmatrix} 45 & 99 & 8 \\ 99 & 38 & 7 \\ 8 & 7 & 40 \end{pmatrix} \text{ (MPa)}$$

##### (d) $\text{Co}_{0.333}\text{Ni}_{0.666}\text{O}$

$$\sigma_{ij} = \begin{pmatrix} 1353 & -56 & -74 \\ -56 & 1198 & 20 \\ -74 & 20 & 1422 \end{pmatrix} \\ \pm \begin{pmatrix} 115 & 15 & 32 \\ 15 & 117 & 11 \\ 32 & 11 & 151 \end{pmatrix} \text{ (MPa)}$$

## Appendix C

### Strain and Stress Tensors Measured and Calculated from Neutron Diffraction Data

#### Strain Tensor for $\text{Co}_{0.5}\text{Ni}_{0.5}\text{O}/\text{ZrO}_2(\text{CaO})$ $\text{Co}_{0.5}\text{Ni}_{0.5}\text{O}$ {222}

$$\varepsilon_{ij} = \begin{pmatrix} 4.19 & 0.13 & -0.53 \\ 0.13 & 0.973 & 0.18 \\ -0.53 & 0.18 & 2.74 \end{pmatrix} \\ \pm \begin{pmatrix} 0.09 & 0.01 & 0.07 \\ 0.01 & 0.07 & 0.05 \\ 0.07 & 0.05 & 0.04 \end{pmatrix} \cdot 10^{-3}$$

Stress Tensor for  $\text{Co}_{0.5}\text{Ni}_{0.5}\text{O}/\text{ZrO}_2(\text{CaO})$   $\text{Co}_{0.5}\text{Ni}_{0.5}\text{O}$  {222}

$$\sigma_{ij} = \begin{pmatrix} 1607 & 11 & -28 \\ 11 & 1145 & 11 \\ -28 & 11 & 1462 \end{pmatrix} \\ \pm \begin{pmatrix} 38 & 2 & 15 \\ 2 & 35 & 11 \\ 15 & 11 & 31 \end{pmatrix} \text{ (MPa)}$$

## References

- <sup>1</sup>K. T. Faber, "Ceramic Composite Interfaces: Properties and Design," *Annu. Rev. Mater. Sci.*, **27**, 499–524 (1997).
- <sup>2</sup>M. Y. He, A. G. Evans, and J. W. Hutchinson, "Crack Deflection at an Interface Between Dissimilar Elastic Materials: Role of Residual Stresses," *Int. J. Solids Struct.*, **31** [24] 3443–55 (1994).
- <sup>3</sup>R. Lakshminarayanan, D. K. Shetty, and R. Cutler, "Toughening of Layered Ceramic Composites with Residual Surface Compression," *J. Am. Ceram. Soc.*, **79** [1] 79–87 (1996).
- <sup>4</sup>C. Hillman, Z. Suo, and F. F. Lange, "Cracking of Laminates Subjected to Biaxial Tensile Stresses," *J. Am. Ceram. Soc.*, **79** [8] 2127–33 (1996).
- <sup>5</sup>T. Mah, T. A. Parthasarathy, and L. E. Matson, "Processing and Mechanical Properties of  $\text{Al}_2\text{O}_3/\text{Y}_3\text{Al}_5\text{O}_{12}$  (YAG) Eutectic Composite," *Ceram. Eng. Proc.*, **11** [9–10] 1617–27 (1990).
- <sup>6</sup>J. Homeny and J. J. Nick, "Microstructure Property Relations of Alumina Zirconia Eutectic Ceramics," *Mater. Sci. Eng., A*, **127** [1] 123–33 (1990).
- <sup>7</sup>Y. Waku, N. Nakagawa, T. Wakamoto, H. Ohtsubo, K. Shimizu, and Y. Kohtoku, "A Ductile Ceramic Eutectic Composite with High Strength at 1873 K," *Nature (London)*, **389** [4 (Sept)] 49–52 (1997).
- <sup>8</sup>C. O. Hulse and J. A. Batt, "The Effect of Eutectic Microstructure on the Mechanical Properties of Ceramic Oxides," N910803-10, United Aircraft Research Laboratories. National Technical Information Service, Springfield, VA, 1974.
- <sup>9</sup>V. S. Stubican and R. C. Bradt, "Eutectic Solidification in Ceramic Systems," *Annu. Rev. Mater. Sci.*, **11**, 267–97 (1981).
- <sup>10</sup>E. C. Dickey, V. P. Dravid, and C. R. Hubbard, "Interlamellar Residual Stresses in Single Grains of NiO– $\text{ZrO}_2$ (Cubic) Directionally Solidified Eutectics," *J. Am. Ceram. Soc.*, **80** [11] 2773–80 (1997).
- <sup>11</sup>E. C. Dickey, C. S. Frazer, T. R. Watkins, and C. R. Hubbard, "Residual Stresses in High Temperature Ceramic Eutectics," *J. Eur. Ceram. Soc.*, **19** [13–14] 2503–509 (1999).
- <sup>12</sup>J. A. Pardo, R. I. Merino, V. M. Orera, J. I. Pena, C. Gonzalez, J. Y. Pastor, and J. Llorca, "Piezospectroscopic Study of Residual Stresses in  $\text{Al}_2\text{O}_3$ – $\text{ZrO}_2$  Directionally Solidified Eutectics," *J. Am. Ceram. Soc.*, **83** [11] 2745–52 (2000).
- <sup>13</sup>L. N. Brewer, V. P. Dravid, G. Dhalenne, and M. Velazquez, "Solid Solution Directionally Solidified Eutectic Oxide Composites: I. Eutectic Growth and Characterization," *J. Mater. Res.*, **17** [4] 760–67 (2002).
- <sup>14</sup>L. N. Brewer, V. P. Dravid, M. Velazquez, and A. Revcolevschi, "Solid Solution Directionally Solidified Eutectic Oxide Composites: II.  $\text{Co}_{1-x}\text{Ni}_x\text{O}$  Single Crystal Growth and Characterization," *J. Mater. Res.*, **17** [4] 768–73 (2002).
- <sup>15</sup>D. E. Smith, T. Y. Tien, and L. H. Van Vlack, "Nickel Oxide–Calcium Oxide System," *J. Am. Ceram. Soc.*, **52** [8] 459–60 (1969).
- <sup>16</sup>E. N. Timofeeva, N. I. Timofeeva, L. N. Drozdova, and O. A. Mordovin, "Reaction of Nickel(II) Oxide with Yttrium Oxide," *Izv. Akad. Nauk SSSR, Neorg. Mater.*, **5** [6] 1155–56 (1969).
- <sup>17</sup>N. Uchida and S. Saito, "Elastic Constants and Acoustic Absorption Coefficients in MnO, CoO, and NiO Single Crystals at Room Temperature," *J. Acoust. Soc. Am.*, **51** [5 (Part 2)] 1602–605 (1971).
- <sup>18</sup>R. P. Ingel and D. Lewis III, "Elastic Anisotropy in Zirconia Single Crystals," *J. Am. Ceram. Soc.*, **71** [4] 265–71 (1988).
- <sup>19</sup>Y. S. Touloukian, "Oxides and Their Solutions and Mixtures"; p. 970 in *Thermophysical Properties of High Temperature Solid Materials*, Vol. 4. Macmillan, New York, 1967.
- <sup>20</sup>E. S. Lukin and D. N. Poluboyarinov, "Some Thermomechanical Properties of Pure Oxide Ceramics," *Refractories (Moscow) (Ogneupory)*, **7**, 318–23 (1963).
- <sup>21</sup>S. P. Terblanche, "Thermal-Expansion Coefficients of Yttria-Stabilized Cubic Zirconias," *J. Appl. Crystallogr.*, **22**, 283–84 (1989).
- <sup>22</sup>S. K. Filatov, V. A. Frank-Kamenetskii, and T. A. Zhuravina, "Thermal Expansion of Zirconium Refractories," *Inorg. Mater. (Neorg. Mater.)*, **5** [2] 346–51 (1969).
- <sup>23</sup>A. G. Karaulov, E. I. Zoz, I. N. Rudyak, and T. E. Sudarkina, "Structure and Properties of Solid Solutions in the Systems:  $\text{ZrO}_2$ – $\text{MgO}$ ,  $\text{ZrO}_2$ – $\text{CaO}$ , and  $\text{ZrO}_2$ – $\text{Y}_2\text{O}_3$ ," *Refractories (Moscow) (Ogneupory)*, **9**, 17–22 (1983).
- <sup>24</sup>*Jade: XRD Pattern Processing*. Materials Data Inc., Livermore, CA, 1999.
- <sup>25</sup>I. C. Noyan and J. B. Cohen, *Residual Stress, Measurement by Diffraction and Interpretation*. Springer-Verlag, New York, 1986.
- <sup>26</sup>W. H. Press, S. A. Teukolsky, W. T. Vetterling, and B. P. Flannery, *Numerical Recipes in Fortran*, 2nd ed. Cambridge University Press, Cambridge, U.K., 1992.
- <sup>27</sup>J. F. Nye, *Physical Properties of Crystals*. Oxford Science Publications, Oxford, U.K., 1985.
- <sup>28</sup>G. E. Bacon, *Neutron Diffraction*, 2nd ed. Clarendon Press, Oxford, U.K., 1962.
- <sup>29</sup>D. P. Woodruff, *The Solid Liquid Interface*. Cambridge University Press, New York, 1973.
- <sup>30</sup>P. Peralta, R. Dickerson, J. R. Michael, K. J. McClellan, F. Chu, and T. E. Mitchell, "Residual Thermal Stresses in  $\text{MoSi}_2$ – $\text{Mo}_5\text{Si}_3$  In-Situ Composites," *Mater. Sci. Eng.*, **A261**, 261–69 (1999).
- <sup>31</sup>E. C. Dickey, V. P. Dravid, P. D. Nellist, D. J. Wallis, S. J. Pennycook, and A. Revcolevschi, "Structure and Bonding at Ni– $\text{ZrO}_2$  (Cubic) Interfaces Formed by the Reduction of a NiO– $\text{ZrO}_2$  (Cubic) Composite," *Microsc. Microanal.*, **3** [5] 443–50 (1997).
- <sup>32</sup>F. Guiberteau, A. Dominguez-Rodriguez, M. Spendel, and J. Castaing, "Plastic Deformation of Bunsenite (NiO) at Temperatures below 1050°C," *Rev. Phys. Appl.*, **21**, 87–92 (1986).
- <sup>33</sup>J. Castaing, M. Spendel, J. Philibert, A. Dominguez-Martinez, and R. Marquez, "Plastic Deformation of CoO Single Crystals," *Rev. Phys. Appl.*, **15**, 277–83 (1980).
- <sup>34</sup>A. Dominguez-Rodriguez, J. Cabrera-Cano, R. Marquez, and J. Castaing, "High-Temperature Creep of Equimolar NiO–CoO Solid Solution," *Phys. Status Solidi*, **85**, 445–47 (1984).
- <sup>35</sup>I. Dutta, "Role of Interfacial and Matrix Creep During Thermal Cycling of Continuous Fiber Reinforced Metal–Matrix Composites," *Acta Mater.*, **48**, 1055–1074 (2000). □